

A COMPACT COPLANAR BROADBAND RECTANGULAR SLOT ANTENNA WITH E-SHAPED FEEDING STRUCTURE FOR GPR APPLICATIONS

F. Sagnard*

Université Paris-Est, IFSTTAR, Department MACS, 58, Bd Lefebvre, 75732 Paris Cedex 15, France

Abstract—A coplanar rectangular slot antenna operating in the very wide frequency band from 0.27 to 3.1 GHz (bandwidth over 166%) has been designed for GPR applications. The antenna, which is supposed to be positioned on the soil surface, appears particularly compact ($34 \times 29 \text{ cm}^2$) and exhibits a low cross-polarization in the E -plane. 3D FDTD simulations have allowed to make a detailed parametric study associated with the antenna dimensional parameters in order to optimize the radiating performances. The slot antenna has also been studied with a shield to be further integrated in a bistatic subsurface radar positioned on the soil surface. Simulated results of the link in the presence of a homogeneous soil then including buried objects met in civil engineering structures are presented and discussed. First experimental results on a sandy soil have been compared to numerical ones.

1. INTRODUCTION

Antennas with broadband characteristics have recently found various applications in modern ultra wide band (UWB) communication systems and in ground penetrating radar (GPR) [1–8]. Our applications are focused on imaging the subsurface of a large range of civil engineering structures at several depths using a bistatic GPR positioned on or close to the ground surface [8–10]. The development of a compact broadband pair of antennas operating in all the frequency band from 0.27 to 3.1 GHz, whose radiation characteristics have been preliminarily studied theoretically in details in different configurations, allows the probing of the subsurface in several frequency sub-bands using a step frequency (SF-GPR) acquisition mode.

Received 29 September 2011, Accepted 4 April 2012, Scheduled 22 April 2012

* Corresponding author: Florence Sagnard (florence.sagnard@ifsttar.fr).

Microstrip patch antennas (MPAs) are one of the most basic and important types of planar antennas because they offer many advantages such as compact size, low-cost, ease of fabrication, light weight, and various shapes design [2, 3]. However, a low bandwidth and a low gain are the main shortcomings for such a planar structure. The microstrip antenna has now reached maturity, and many techniques have been suggested for achieving a high bandwidth such as using more complex shapes, parasitic elements, multilayer configurations and the tuning of the feed line [11–14]. In this paper, an original printed rectangular slot antenna fed by a $50\ \Omega$ CPW (coplanar waveguide) transmission line tuned by a E-shaped patch is presented [13, 14]. Presently, little work has been done to lower the operating frequency band of microstrip antennas at frequencies less than 0.8 MHz and to reduce the antenna size at these frequencies because major applications concern UWB wireless communications. The main concern of this study is to rely on recent developments in coplanar technology associated with ultra wide band (UWB) or broad band antennas to design a compact ($34 \times 29\ \text{cm}^2$) antenna operating at a frequency as low as 0.27 GHz, thus quite lower than 1 GHz [2, 3]. By choosing a relative combination of a E-shaped patch, a linear feed line and a rectangular slot, we have designed an antenna structure on a FR4 substrate ($h = 1.5\ \text{mm}$) with a very wide operating bandwidth whose nearly half of the spectrum covers frequencies lower than 1 GHz. A partial shield, only opened towards the ground and coated with an inner layered absorbing material, has been added to eliminate undesirable reflections from the upper environment particularly at low frequencies; moreover, in a GPR system, the antenna shielding will allow to reduce the coupling between the transmitting and the receiving units [9].

In this paper, the proposed broadband rectangular slot antenna has been simulated using the 3D commercial software EMPIRE (distributed by IMST) based on the finite difference time domain (FDTD) technique. A first detailed parameter study done in air has allowed to define the several geometrical parameters of the unshielded slot antenna, which are the result of a compromise on the frequency bandwidth (reflection coefficient $S_{11} < -10\ \text{dB}$) and compact dimensions. Afterwards, the antenna radiation characteristics have been studied in the presence of a shield (conductive box coated with a multi-layered lossy material) and a common soil ($\epsilon' = 5.5$; $\sigma = 0.01\ \text{S} \cdot \text{m}^{-1}$). A pair of antennas has then been considered to form a bistatic radar link positioned on the soil surface, where the soil can include buried objects met in civil engineering structures; the antenna offset has been particularly studied to highlight the influence of the antenna coupling on the detection of a buried pipe or a crack.

2. ANTENNA STRUCTURE AND DESIGN

2.1. Antenna Structure

The geometry of the proposed rectangular slot ($L_1 = 270$ mm; $W_1 = 165$ mm) antenna with all its parameters is shown in Figures 1(a) and 1(b). The antenna has been designed on a classical single-sided FR4 ($\epsilon'_r = 4.4$; $\tan \delta = 0.01$) substrate, with thickness $h_s = 1.5$ mm. The patch size is characterized by a length $W_s = 288.5$ mm and a width $L_s = 340$ mm. The rectangular slot is excited by a CPW feed-line with a characteristic impedance 50Ω whose length is $l = 77$ mm; the CPW transmission line itself is formed by a conductive strip with a width $b = 3$ mm and a gap distance $a = 0.4$ mm between the strip and the coplanar ground plane. The two finite ground planes are placed symmetrically at both sides of the CPW line. The E-shaped tuning patch and its relative position in the rectangular aperture strongly influences the S_{11} frequency variations. Moreover, the associated trident feed line has allowed to significantly increase the bandwidth beyond frequencies greater than 1 GHz. The trident feed line has a lower width than the CPW line with $b' = 2$ mm. The 3D simulations of the antenna under the commercial software EMPIRE, based on the FDTD approach, have allowed to perform a detailed parametric study associated with the geometrical elements to obtain a return loss $S_{11} < -10$ dB in the frequency band of 0.27 to 3.1 GHz. The influence of main parameters such as W_2 ; W_4 ; L_2 ; L_3 ; L_4 ; c and the trident feed line are reported. Afterwards, the far-field radiation patterns associated with fields E_θ and E_φ corresponding to the co-polar and cross-polar components in both planes E -plane (x - z) and H -plane (y - z) are presented at several frequencies in air.

The radiation of the rectangular slot antenna (field modes), which is initially a narrow band antenna, has been described by the cavity model [3]. The fringing effect induced at the open side walls produces radiation along the antenna width W_1 ; however in our case, we have verified that this effect appears negligible (0.53% for f_{10}). The introduction of a tuning stub inside the slot has allowed to create a very broad impedance bandwidth. The resonant frequency f_{mn} of the excited mode TM_{mn} is obtained using the following relation [3]:

$$f_{mn} = \frac{c}{2\sqrt{\epsilon'_e}} \left[\left(\frac{m}{L_1} \right)^2 + \left(\frac{n}{W_1} \right)^2 \right]^{1/2} \quad (1)$$

where ϵ'_e is the effective real permittivity.

Thus, according to the dimensions of the slot antenna, the effective permittivity is $\epsilon_e = 4.32$ and the fundamental mode TM_{10} leads to the

lower resonant frequency $f_{10} = 265.6$ MHz. The 3 following frequency modes ($L/W = 1.64$) are $f_{01} = 437$ MHz, $f_{20} = 534.1$ MHz and $f_{21} = 690.1$ MHz.

The current distribution on the antenna surface has been calculated by numerical simulations; the results visualized in Figure 2 at the frequency 560 MHz highlight that the trident-shaped feed line provides the alignment of the surface current j_{xy} in the patch along the $0x$ axis in a quasi uniform distribution [14].

2.2. Parametric Study Associated with the Geometry

The influence of main geometrical parameters on the return loss S_{11} of the rectangular slot antenna in air are now detailed. This study allows to justify the final dimensions defined in Figure 1.

Firstly, the trident-shaped feed has been studied. As shown in Figure 3(a), the trident-shaped feed considerably increases the bandwidth ($S_{11} < -10$ dB) of the antenna to the upper frequency

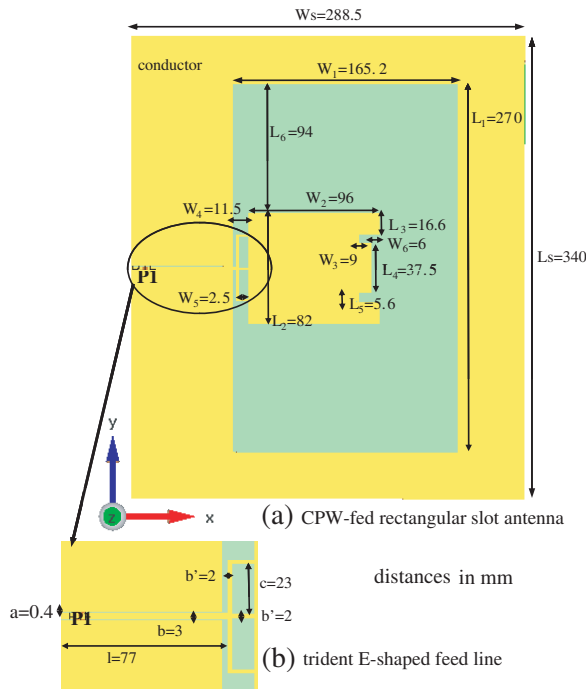


Figure 1. Geometry of the proposed CPW and E-shaped fed rectangular slot antenna. (a) General top view and (b) top view of the trident E-shaped feed line (all distances are in mm).

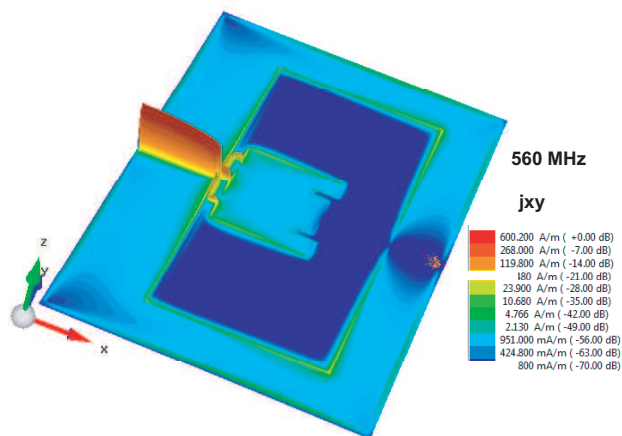


Figure 2. Current distribution j_{xy} of the surface of the rectangular slot antenna at frequency 560 MHz (incident pulse current 0.2 A, and duration 0.52 ns).

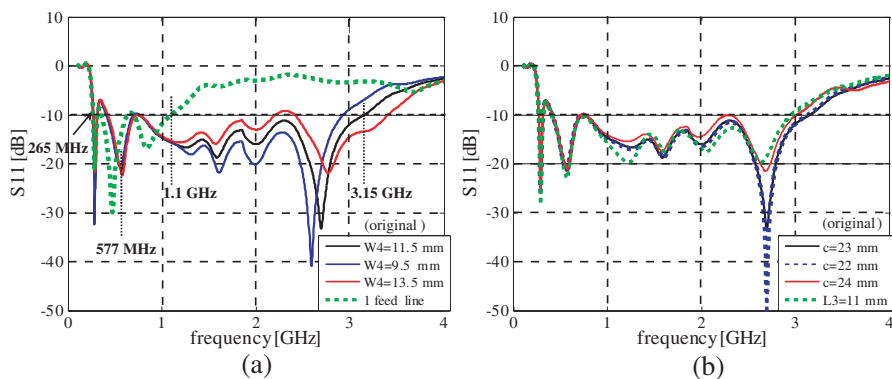


Figure 3. Return loss S_{11} (dB) of the rectangular slot antenna in air (a) for various W_4 values and feed line structures, and (b) various c and L_3 values.

3.1 GHz comparing to 1.1 GHz which is reached where only one feed line is used (with the characteristics of the CPW line). Moreover, we have remarked from results in Figure 3(a) that the distance W_4 , between the slot frontier and the E-shaped patch strongly influences the S_{11} amplitude at frequencies higher than 1.1 GHz and also the upper bandwidth limit; considering W_4 values ranging from 9.5 to 13.5 mm, the value $W_4 = 11.5$ mm appears as the best compromise on

the frequency bandwidth and the return loss amplitude. In Figure 3(b), the study of the influence distance c between each parallel feed lines ranging from 22 to 24 mm shows that it affects the S_{11} amplitude and the upper bandwidth limit; thus, the value $c = 23$ mm has been fixed. The height L_3 of the upper element of the E-patch shows from Figure 3(b) that it influences the bandwidth at the higher frequencies and the S_{11} amplitude; consequently, the value $L_3 = 16.6$ mm has been defined. Afterwards, the influence of the dimensions (L_2 ; W_2) of the E shaped patch has been studied. From Figure 4(a), we remark that in the range 76 to 88 mm, the height L_2 influences the S_{11} amplitudes for frequencies higher than 0.85 GHz and also the upper bandwidth limit; we have defined the optimum value to 82 mm to obtain S_{11} amplitudes clearly less than -10 dB around 2.3 GHz. From Figure 4(b), we observe that parameter W_2 influences significantly S_{11} amplitudes at frequencies ranging from 0.29 to 2.4 GHz and slightly the upper bandwidth; the value $W_2 = 96$ mm appears to be the optimum solution.

The radiation patterns associated with the E -field (co-polarisation and cross-polarisation), in both planes, E -plane ($\phi = 0^\circ$; xOz) and H -plane ($\phi = 90^\circ$; yOz), and expressed in terms of the total gain (including ohmic and reflection losses $|S_{11}|^2$) are presented in Figure 5 for four frequencies 0.3, 1, 2, and 2.8 GHz. In the E -plane, we generally remark that there is quite low cross polarization between both E -field components E_θ and E_φ ; the gain is evaluated to 3.25 dB at 0.3 GHz, 6 dB at 1 GHz, 2.4 dB at 2 GHz, and 1.31 dB at 2.8 GHz. A maximum gain is thus observed around 1 GHz, and the weak gain for this slot antenna is a priori due to the compact size of the antenna, its very

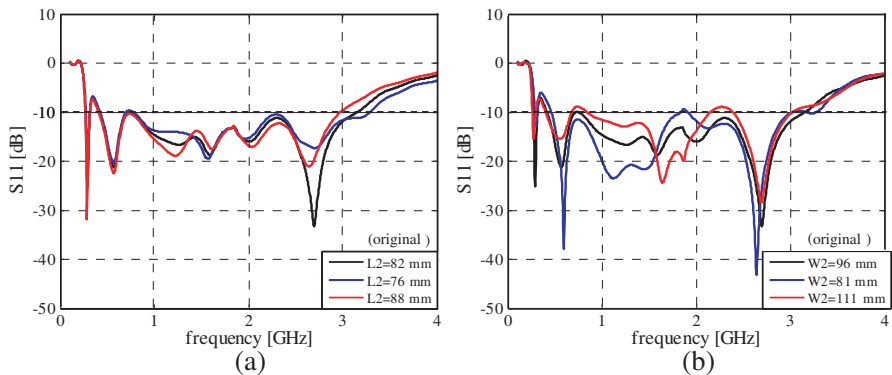


Figure 4. Return loss S_{11} (dB) of the rectangular slot antenna in air (a) for various L_2 values, and (b) W_2 values.

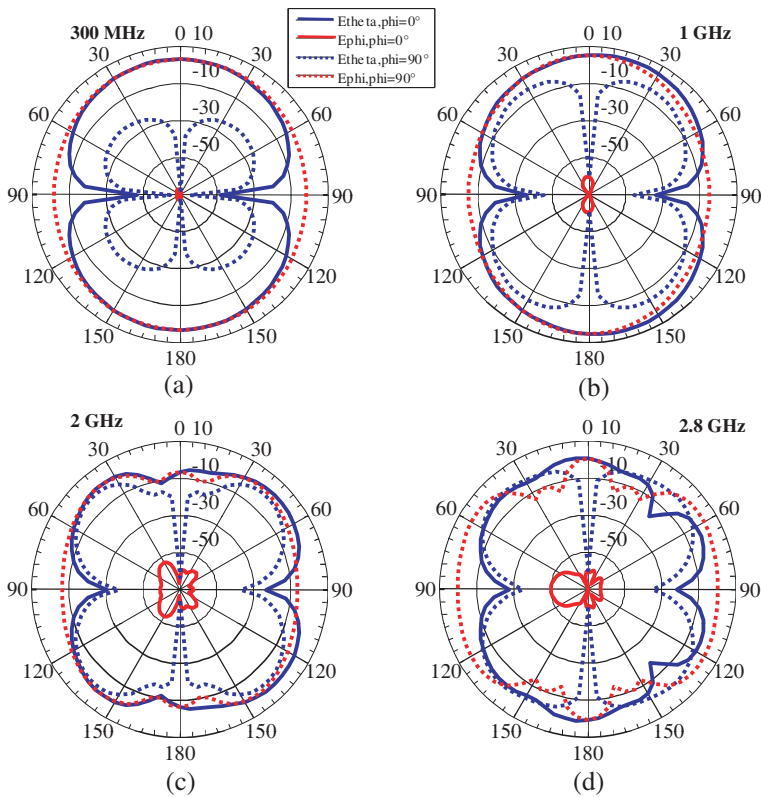


Figure 5. Far-field radiation patterns (E_θ and E_ϕ , losses included) in air of the rectangular slot antenna without shield in the E -plane (xOz) and H -plane (yOz) at 0.3, 1, 2 and 2.8 GHz.

wide frequency band and the high permittivity of the substrate. The gain could be improved using several approaches synthesized in [15], and it will be the second objective of this work, as the first one was to show that a quite compact slot antenna operating at low frequencies can be designed using the microstrip technology. In the H -plane, we remark that the minimum cross-polarisation between both E -field components is evaluated to 4.8 dB. At 2 GHz and higher, the amplitudes of both E -field components appear very close, and at these frequencies electromagnetic waves will not penetrate a soil. At 1 GHz, the maximum gain obtained for the component E_ϕ is evaluated to 5.4 dB.

2.3. Effect of a Partial Shield

When designing a radar system supposed to be positioned parallel to the ground surface, it appears necessary to eliminate the backward radiations in air induced by the environment, and to reduce significantly the direct coupling between the transmitting and the receiving antennas. According to previous studies [9, 16], a rectangular shield formed of a perfectly conductive box and coated by an inner flat absorbing material has been added. In general, the dielectric characteristics of commercial absorbers are not known for confidential reasons, and approximate models are made. A characterization in reflection is generally made to extract the reflection coefficient of each absorbing layer to extract the complex permittivity and the permeability as a function of the frequency. Our model is based on Atteia's simple model [9] which has considered a conductivity profile to reduce sharp reflections at the cavity frontiers. We have previously used this model [16] and observed that S_{11} bandwidth remains unchanged as compared to the unshielded case, and also that theoretical and numerical results compare satisfactorily.

In this work, we have considered a flat absorbing material (called Radar Absorbing Material RAM) made of three layers with a low dielectric constant $\varepsilon_{1,2,3} = 1.5$. As visualized in Figure 6, the antenna shield has the following width length and height $h_c = 356.5$ mm, $L_c = 432$ mm, and $h_c = 76.5$ mm ($e_1 + e_2 + e_3$). The RAM shows an

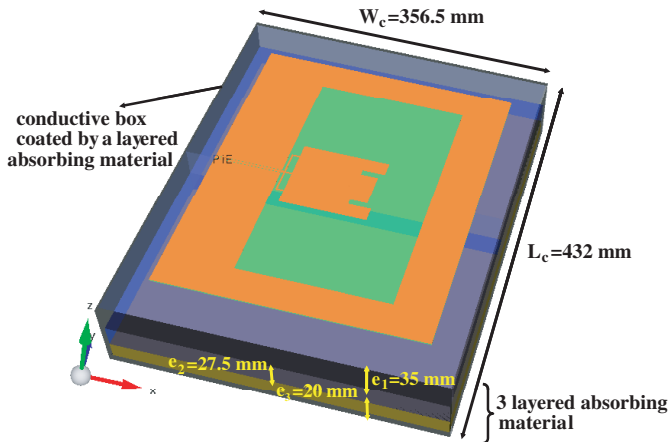


Figure 6. Structure of the proposed rectangular slot antenna shielded and including inner walls coated with a three-layered absorbing material.

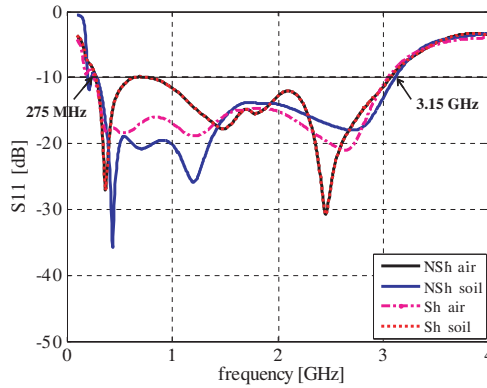


Figure 7. Return loss S_{11} (dB) of the rectangular slot antenna in air and in the presence of a common soil ($\epsilon'_s = 5.5$; $\sigma_s = 0.01 \text{ S} \cdot \text{m}^{-1}$, elevation $h = 10 \text{ mm}$) with or without a shield.

increasing conductivity profile from the antenna patch to upper part of the box such as: $\sigma_1 = 0.01 \text{ S} \cdot \text{m}^{-1}$; $e_1 = 35 \text{ mm}$; $\sigma_2 = 0.1 \text{ S} \cdot \text{m}^{-1}$; $e_2 = 27.5 \text{ mm}$ and $\sigma_3 = 1 \text{ S} \cdot \text{m}^{-1}$; $e_3 = 20 \text{ mm}$. We have shown that with this model a minimum box height of 76.5 mm is necessary to affect weakly the S_{11} amplitude. Moreover, weak variations of the several layer thicknesses do not significantly modify the S_{11} plot. All the antenna structure has been simulated under EMPIRE in two configurations: in the presence of air and of a half-space common soil ($\epsilon'_s = 5.5$; $\sigma_s = 0.01 \text{ S} \cdot \text{m}^{-1}$) at an elevation $h = 10 \text{ mm}$ (to consider potential irregularities on the soil surface). The S_{11} amplitude variations presented in Figure 7 show that in air the shield does not bring modifications. However, in air the presence of a shield produces a S_{11} amplitude higher in the frequency range $[0.37; 1.3] \text{ GHz}$. On top of a common soil ($h = 10 \text{ mm}$), the shielded antenna appears more matched than in air as the S_{11} amplitude in the bandwidth appears lower than -15 dB . In general, we observe that the shield smoothes the return loss response and does not change the bandwidth. The associated impedance variations (real and imaginary parts) versus frequency and plotted in Figures 8(a) and 8(b) for a shielded antenna in air and a presence of a soil confirm that the soil contributes to smooth the variations; in the bandwidth, the real part varies between 26.7 and 89.3 Ω , and between 39.3 and 72.3 Ω .

The radiation patterns of the shielded antenna in air at four frequencies 0.3, 1, 2, and 2.8 GHz are plotted in Figure 9. In general, we remark that the shield induces an attenuation greater than 20 dB in the backward direction and modifies slightly the maximum gain.

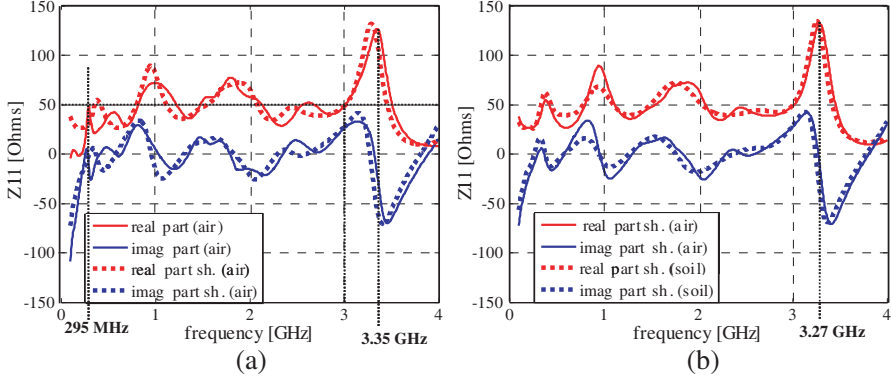


Figure 8. Complex impedance of the rectangular slot antenna shielded in air and in the presence of a common soil ($\varepsilon'_s = 5.5$; $\sigma_s = 0.01 \text{ S} \cdot \text{m}^{-1}$, elevation $h = 10 \text{ mm}$), (a) real and (b) imaginary parts.

3. RADAR SYSTEM

3.1. Homogeneous Soil

The radar system, modeled under EMPIRE and visualized in Figure 10(a), is made of a pair of transmitting (50Ω) and receiving ($10 \text{ k}\Omega$) rectangular shielded slot antennas positioned parallel to a semi infinite common homogeneous soil ($\varepsilon'_s = 5.5$; $\sigma_s = 0.01 \text{ S} \cdot \text{m}^{-1}$) in the mirror configuration at an elevation $h = 10 \text{ mm}$. Firstly, the influence of the distance d between both antennas on the transmission coefficient S_{21} (dB) has been studied (see Figure 10(b)) to define the offset resulting from a compromise between a weak direct path amplitude (low S_{21}) and a sufficient high signal amplitude containing soil information. When changing the offset between both antennas from 60 to 140 mm with a step of 20 mm, we observe from Figure 10c weak amplitude differences at frequencies lower than 500 MHz. Moreover, we remark that the coefficient S_{21} associated with the surface wave (direct path) induces an amplitude lower than -53 dB in the frequency band 0.1 to 4 GHz. The offset 100 mm which have been defined appears reasonable as it will allow to detect objects buried at the depth 120 mm with a marked amplitude in the time domain (see Figures 12 and 13); in this case, the maximum direct wave amplitude is less than 5.3 mV. Because the antennas are positioned very close to the soil surface, we consider that the direct wave propagates at a velocity v_{av} which is an

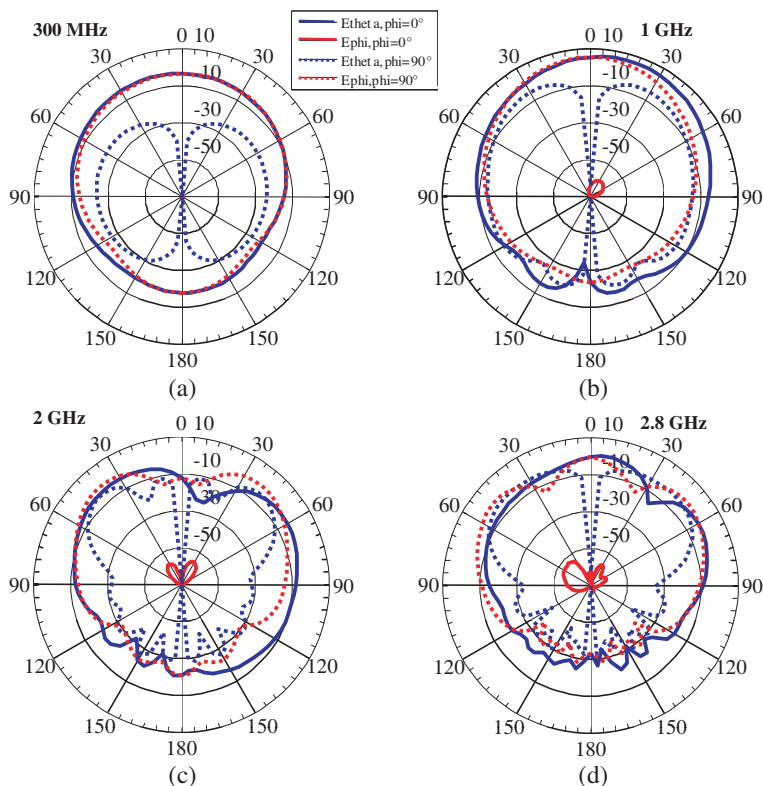


Figure 9. Far-field radiation patterns (E_{θ} and E_{φ} , losses included) in air of the rectangular slot antenna shielded in the E -plane (xOz) and H -plane (yOz) at 0.3, 1, 2 and 2.8 GHz.

average of the velocity in air (c) and in the soil ($c/\sqrt{\epsilon'_s}$) such as:

$$v_{av} = \frac{1}{2} \left(c + \frac{c}{\sqrt{\epsilon'_s}} \right) \tag{2}$$

Thus, the first arrival time (offset = 100 mm) is evaluated analytically to 3.47 ns which is confirmed by the numerical results collected in Figure 10(b).

Then, the influence of the elevation h studied in Figure 11 shows that the amplitude of the direct path is greatly increased when the antennas are put on the soil surface (factor 6), thus the coupling between both antennas in the presence of the soil appears significative.

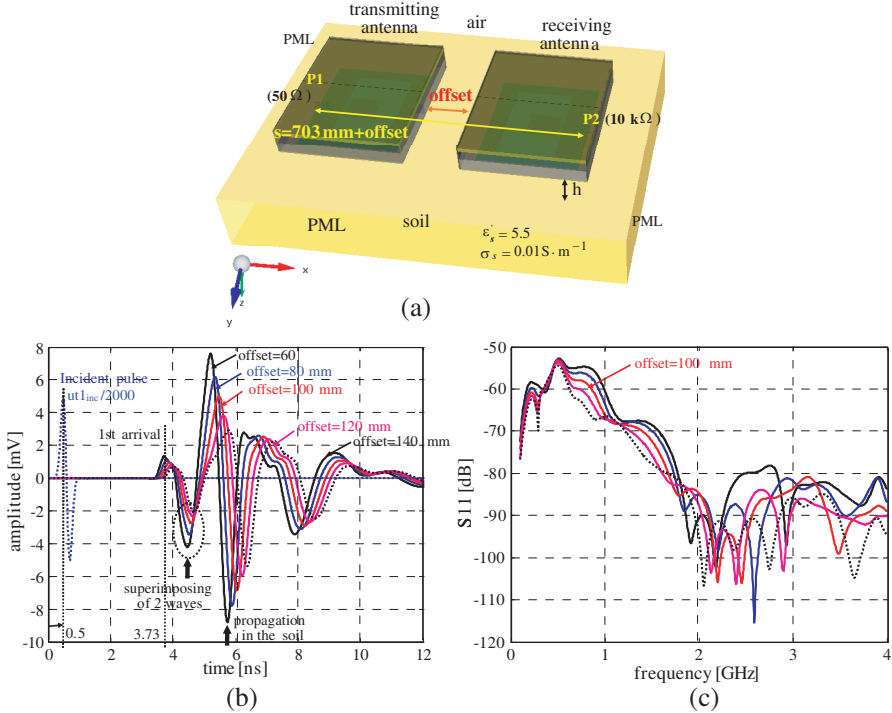


Figure 10. FDTD simulations in the parallel configuration. (a) Geometry of the radar system above a common soil ($\epsilon'_s = 5.5$; $\sigma_s = 0.01 \text{ S} \cdot \text{m}^{-1}$) at an elevation h (all distances are in mm), (b) time signal at Port 2 for different values of the offset, and (c) the associated transmission coefficient S_{21} (dB).

3.2. Soil with Buried Objects

Then, two types of objects, a dielectric ($\epsilon'_{\text{diel}} = 3.4$ thickness 1 mm) pipe with a radius 100 mm and a vertical crack with width 52 mm, both filled with air have been buried in the common homogeneous soil ($\epsilon'_s = 5.5$; $\sigma_s = 0.01 \text{ S} \cdot \text{m}^{-1}$) as shown in Figures 12(a) and 12(b) respectively. The depth e of the objects in the soil is 120 mm. The excitation signal has the shape of the first derivative of the gaussian function with a duration $w = 0.5 \text{ ns}$; its frequency spectrum is centered at 1 GHz, and the bandwidth is 3 GHz on both sides from this center frequency. In the arrival time calculations, the distance between the antennas at ports P_1 and P_2 ($s = 703 \text{ mm} + \text{offset}$) has to be considered.

As the path $2L$ associated with the reflected path on a buried object (see Figure 12(c)) appears significantly greater than the

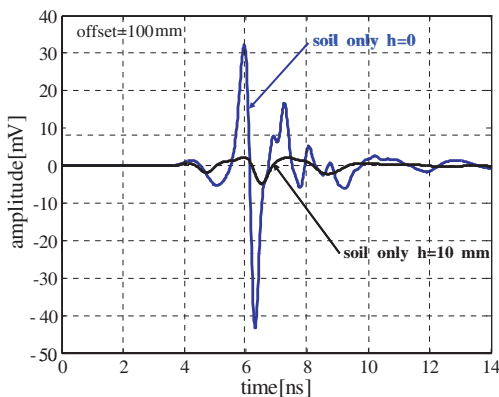


Figure 11. Time signal at Port 2 for two elevation distances $h = 0$ and 10 mm above the common soil ($\epsilon'_s = 5.5$; $\sigma_s = 0.01 \text{ S} \cdot \text{m}^{-1}$, offset = 100 mm).

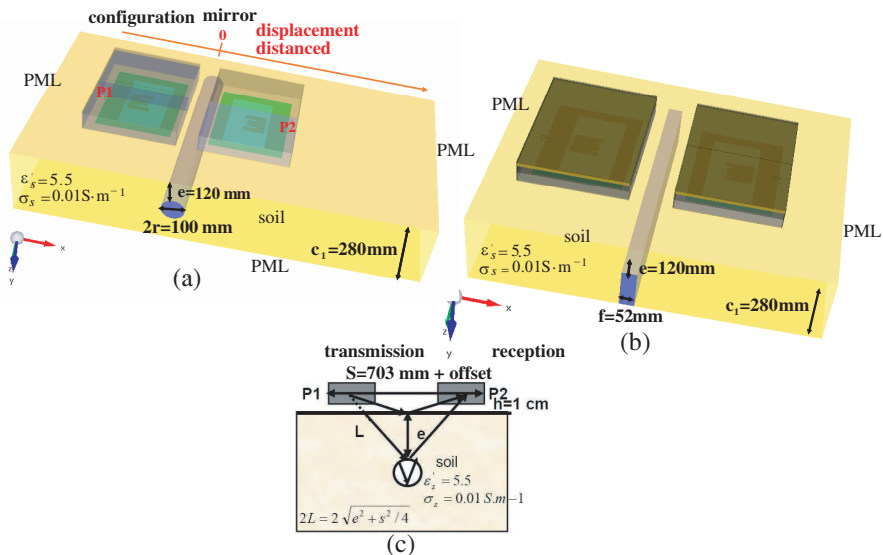


Figure 12. The radar system in the presence of buried objects at 120 mm under the soil surface, (a) a PVC pipe with diameter 10 cm filled with air, and (b) a 5 cm width crack filled with air with an infinite height. (c) Scheme of the wave paths generated by a radar system in a soil with a buried pipe.

elevation h ($h \ll 2L$), we can consider the following relation to analyze the several time waveforms

$$2L = 2 \sqrt{e^2 + s^2/4} \tag{3}$$

$$t_1 = \frac{2L}{v_{\text{soil}}}; \quad v_{\text{soil}} = \frac{c}{\sqrt{\epsilon'_s}} \tag{4}$$

Thus, the propagation time t_1 is estimated to be 6.9 ns using the analytical relations (3) and (4) if we consider the distance between ports $s = 743$ mm (offset = 100 mm); in this configuration, if the distance between antenna centers is $s_{\text{center}} = 494.5$ mm, the propagation time t_1 is evaluated to be 5.62 ns, thus very close to 5.67 ns calculated from numerical simulations (see Figure 13(a)). Because the pipe depth appears small as compared to the antenna distance s , we observe in Figure 13(a) an overlap of two wave components around 6 ns associated with the direct wave propagating in the soil and the reflected wave from the dielectric pipe. Both signals associated with the pipe and the crack appear similar. However the signal corresponding to the crack appears about twice weaker, and its width is twice weaker as the pipe diameter. It must be mentioned that the crack has a semi-infinite extent in depth. In general, we remark that the direct waves generated in the presence of a homogeneous soil show very low amplitudes as compared to the wave reflected by the buried object. The displacement of the radar system on the soil

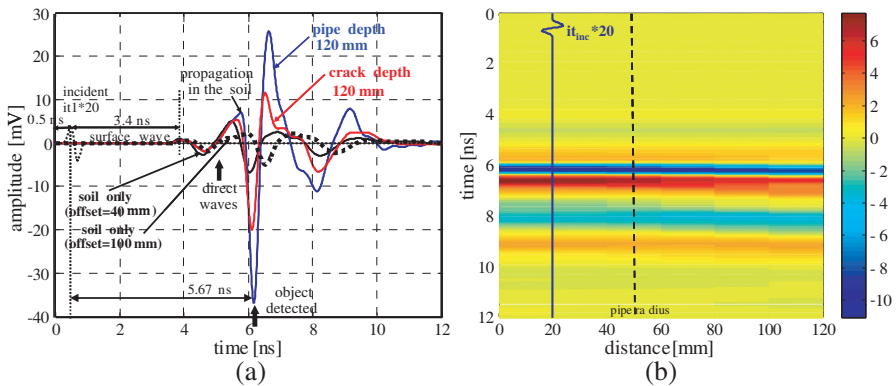


Figure 13. Time signals at Port 2 issued from the buried objects in the common soil ($\epsilon'_s = 5.5$; $\sigma_s = 0.01 \text{ S} \cdot \text{m}^{-1}$). (a) Comparison of the configurations including a buried pipe and a buried crack all filled with air, and (b) radargram (scan along Ox with fixed offset = 100 mm) associated with the case of the buried pipe.

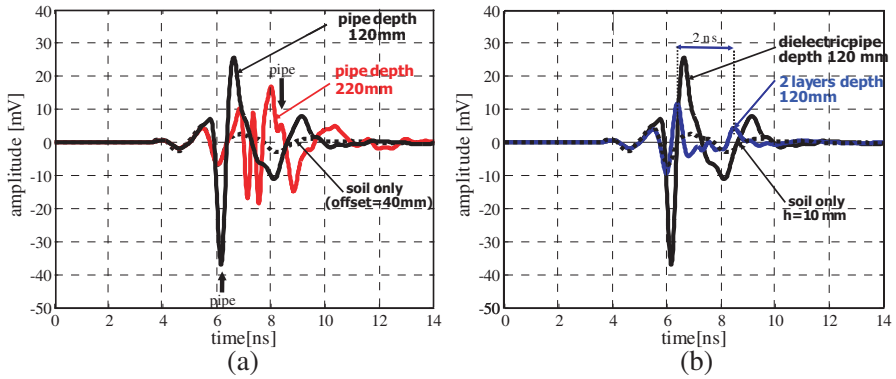


Figure 14. Time signals at Port 2 issued from several configurations. (a) Several pipe depths 120 and 220 mm, and (b) a pipe at depth 120 mm and a two-layered soil (layer 1 $e_1 = 120$ mm, $\epsilon'_1 = 5.5$; $\sigma_1 = 0.01$ S \cdot m $^{-1}$, and layer 2 $e_2 \rightarrow \infty$, $\epsilon'_2 = 9$; $\sigma_2 = 0.01$ S \cdot m $^{-1}$) with an interface at the depth 120 mm.

surface at a fixed offset (offset = 100 mm) along the direction Ox (B-scan) gives a radargram; considering the homogeneous soil with the buried pipe (offset = 100 mm, $e = 120$ mm, $h = 10$ mm), the radargram presented in Figure 13(b) shows part of the hyperbola (the shape of the incident signal has been plotted). Afterwards, the same pipe has been buried 100 mm deeper, thus 220 mm under the soil surface, and we have compared in Figure 14(a) the waveforms at both depths. Considering the distance between antenna centers $s_{\text{center}} = 494.5$ mm, the propagation time t_1 is evaluated to be 7.9 ns; a marked peak can be visualized in Figure 14(a) close to the time 8 ns. The signal before corresponds to the reflection between the antenna shields. Afterwards, a double layered soil has been considered with the following characteristics associated with the thicknesses and the complex permittivities: layer 1, $e_1 = 120$ mm, $\epsilon'_1 = 5.5$; $\sigma = 0.01$ S \cdot m $^{-1}$, and layer 2 $e_2 \rightarrow \infty$, $\epsilon'_2 = 9$; $\sigma = 0.01$ S \cdot m $^{-1}$. The time difference between successive signals reflected on the interface between both layers is theoretically 1.9 ns, which corresponds to the signals observed in Figure 14(b).

4. MEASUREMENTS

Validation measurements have been made on a large wood box such as visualized in Figure 15(a). The wood box with width $l = 1$ m

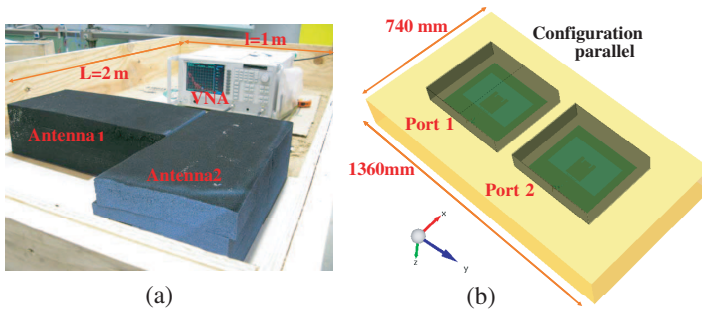


Figure 15. (a) Picture of the experimental setup in a wood box filled with 74 cm height sand coming from the Seine valley, and (b) geometry of the radar system in the parallel configuration that has been used for the FDTD simulations.

and length $L = 2$ m has been filled with a slightly humid and non-compacted sand coming from the Seine valley in France with a height of 74 cm. The measurements have been made using the vector network analyzer (VNA) ANRITSU MS4624B in the frequency band 50 MHz to 5 GHz. A full two ports calibration has been made with 3.5 mm radiofrequency coaxial cables. We have considered 1601 measurement points and a resolution bandwidth of 300 Hz. The antennas have been shielded using commercial planar five-layered absorbing materials. For practical reasons, the parallel configuration of the antenna system such as that presented in Figure 15(b) has first been studied. For the comparison between measurements and simulations, the numerical results involve a common soil $\epsilon'_s = 5.5$; $\sigma_s = 0.01 \text{ S} \cdot \text{m}^{-1}$.

Firstly, considering an offset = 100 mm and an elevation $h = 10$ mm, we have compared the transmission between the pair of shielded antennas for three configurations: mirror, non-mirror, and parallel. The different frequency variations of S_{21} in Figure 16 show higher amplitudes at frequencies greater than 1 GHz for the non mirror configuration. The S_{21} amplitude of the mirror configuration decreases more regularly than the parallel configuration; the slope of the decrease appears similar.

Afterwards, considering the parallel configuration, we have compared measurement and simulation results for both coefficients S_{11} and S_{21} in the frequency band from 0.1 to 4 GHz in Figures 17(a) and 17(b), respectively. In Figure 17(a), the peaks and hollows of the measurements agree satisfactorily with the simulations; the measurement variations versus frequency appear smoother. The S_{11} variations of a slot bow-tie antenna previously developed [16] have

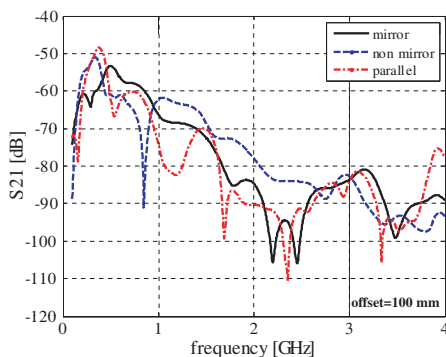


Figure 16. Theoretical transmission coefficient S_{21} (dB) versus frequency for three radar configurations in the presence of a common soil ($\epsilon'_s = 5.5$; $\sigma_s = 0.01 \text{ S} \cdot \text{m}^{-1}$, offset = 100 mm): mirror, non mirror and parallel.

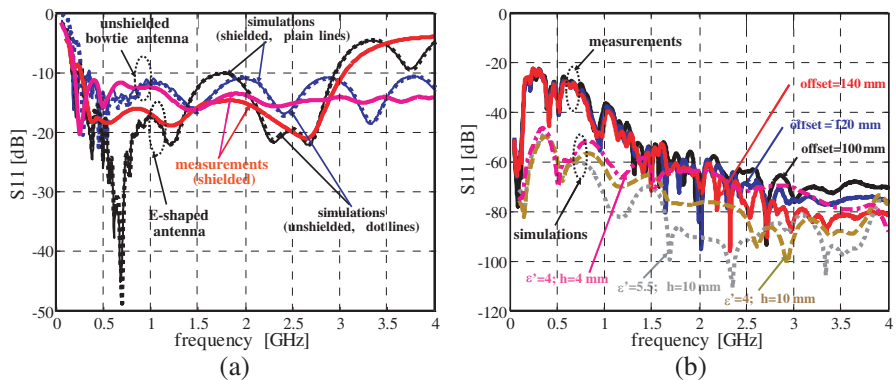


Figure 17. Comparison between measurements and simulations in the presence of a homogeneous soil ($\epsilon'_s = 5.5$; $\sigma_s = 0.01 \text{ S} \cdot \text{m}^{-1}$). (a) Return loss S_{11} (dB) considering a shielded and an unshielded rectangular slot antenna and an unshielded bowtie slot antenna, and (b) transmission coefficient S_{21} (dB) of the shielded rectangular slot antenna for different offsets in the parallel configuration.

been added to Figure 17(a) for comparison because the frequency band appears very similar. Nevertheless, the bow-tie antenna has a wider bandwidth at higher frequencies. The slot bow-tie antenna has a much longer length, and it can be shown from these results that it is possible to design a smaller antenna with a different shape to

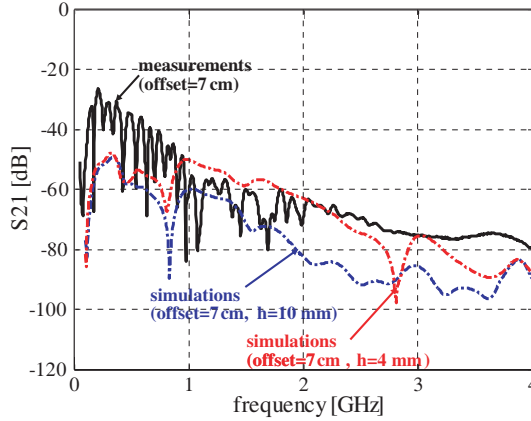


Figure 18. Theoretical and experimental transmission coefficient S_{21} (dB) of the shielded rectangular slot antenna in the non mirror configuration ($\varepsilon'_s = 5.5$; $\sigma_s = 0.01 \text{ S} \cdot \text{m}^{-1}$).

operate at frequencies useful for GPR applications. The comparison between measurements and simulations for the transmission coefficient S_{21} presented in Figure 17(b) show a marked amplitude difference (around 20 dB) at frequencies less than 1 GHz. This can be explained by the shielding of the antenna that was not complete during the measurements as no conductive box has been used for each antenna or by the curved shape of the cables connected to the VNA because of their short length. However, we remark from simulation results in Figure 17(b) that a soil with a lower permittivity $\varepsilon'_s = 4$ ($\sigma_s = 0.01 \text{ S} \cdot \text{m}^{-1}$), that a priori better corresponds to the sand studied [16], significantly increases the S_{21} amplitude at frequencies higher than 0.8 GHz. Moreover, as during the experiments both antennas have been positioned at a weaker elevation than 10 mm, around 4 mm, we notice from the simulations that a lower height produces an increase in the S_{21} amplitude and particularly at frequencies higher than 0.6 MHz. Moreover, we remark that a weaker elevation induces a lower decreasing slope as a function of the frequency. Finally, S_{21} measurements have been made in the non mirror configuration for an offset around 7 cm. The measurements compared to simulation results ($\varepsilon'_s = 4$; $\sigma_s = 0.01 \text{ S} \cdot \text{m}^{-1}$) with two elevations $h = 4$ and 10 mm are presented in Figure 18. As previously, we observe a marked amplitude difference at frequencies less than 0.8 MHz. We remark that the elevation appears between 4 and 10 mm when considering the shape of frequency variations.

5. CONCLUSION

This paper has presented the simulation results associated with the broadband characteristics of an original rectangular slot antenna. The antenna is original as it has relatively short dimensions ($34 \times 29 \text{ cm}^2$) to operate at a frequency as low as 0.27 GHz until 3.1 GHz. A low cross polarization in the E -plane in the overall frequency band characterizes this antenna. Its gain is typical of microstrip antennas and could be improved. A detailed parametric study based on FDTD simulations has allowed to define its geometry which results from a suitable compromise on the feed line, the E-shaped patch, the tuning of the feed line, and the rectangular slot. The modeling of a radar system positioned close to the soil has been made in three different configurations to study in particular the coupling between both antennas through air and the soil. Afterwards, the presence of a buried object (pipe or crack all filled with air) has been considered to show the ability of the system to detect an object surrounded by a dielectric soil. Further studies will be focused on measurement campaigns in several environments (laboratory and controlled place) and the development of data processing to extract quantitative information from radar scans in different frequency sub-bands.

REFERENCES

1. Zhong, S., X. Yan, and X. Liang, "UWB planar antenna technology," *Front. Electr. Electron. Eng.*, Vol. 3, No. 2, 136–144, China, 2008.
2. Wong, K. L., *Compact and Broadband Microstrip Antennas*, 1st edition, John Wiley Sons, 2002.
3. Kumar, G. and K. P. Ray, *Broadband Microstrip Antennas*, Artech House, 2003.
4. James, J. R. and P. S. Holl, "Handbook of microstrip antennas," *IEE Electromagnetic Wave Series*, 1969.
5. Oppermann, I., M. Hamalainen, and J. Iinatti, *UWB Theory and Applications*, John Wiley & Sons, 2004.
6. Daniels, D. J., *Ground Penetrating Radar*, 2nd edition, The IEE, London, 2004.
7. Orlando, L., A. Pezone, and A. Colucci, "Modeling and testing of high frequency GPR data for evaluation of structural deformation," *NDT & E International*, Vol. 43, 216–230, 2010.
8. Capizzi, P. and P. L. Cosentino, "GPR multi-component data analysis," *Near Surface Geophysics*, Vol. 6, 87–95, 2008.

9. Atteia, G. E., A. A. Shaalan, and K. F. A. Hussein, "Wideband partially-covered bowtie antenna for ground-penetrating radars," *Progress In Electromagnetics Research*, Vol. 71, 211–226, 2007.
10. Diamanti, N., D. Redman, and A. Giannopoulos, "A study of GPR vertical crack responses in pavement using field data and numerical modelling," *13th Int. Conf. Ground Penetrating Radar (GPR)*, Jun. 2010.
11. Liu, J., D. Zhao, and B.-Z. Wang, "A beveled and slot-loaded planar bow-tie antenna for UWB applications," *Progress In Electromagnetics Research M*, Vol. 2, 37–46, 2008.
12. Shagar, A. C. and R. S. D. Wahidabanu, "New design of CPW-fed rectangular slot antenna for ultra wideband applications," *Int. Journal Electronics Engineering*, Vol. 2, No. 1, 69–73, 2010.
13. Dastranj, A. and M. Biguesh, "Broadband coplanar waveguide-fed wide-slot antenna," *Progress In Electromagnetics Research C*, Vol. 15, 89–101, 2010.
14. Bayderkhani, R. and G. R. Dadashzadeh, "Printed wideband CPW-fed slot antenna with high polarization purity," *IEICE Electronics Express*, Vol. 7, No. 4, 295–301, 2009.
15. Malaker, K., S. M. Danish Abbas, S. Banerjee, and S. Chattopadhyay, "Microstrip radiating structures: Improved gain and broader band width," *International Journal of Electronics Engineering*, Vol. 3, No. 2, 209–212, 2011.
16. Sagnard, F. and F. Rejiba, "Wide band coplanar waveguide-fed bowtie slot antenna for a large range of ground penetrating radar applications," *IET Microwaves, Antennas and Propagation*, Vol. 5, No. 6, 734–739, 2011.